Dalton Transactions

ROYAL SOCIETY OF CHEMISTRY

PAPER

View Article Online
View Journal | View Issue

Cite this: *Dalton Trans.*, 2023, **52**, 394

Tweaking the bridge in metallocene Zr(IV)/W(IV) bimetallic hydrides†

Selwin Fernando, ‡[a] Martina Landrini,‡[b] Alceo Macchioni, [b] David L. Hughes, [a] Peter H. M. Budzelaar *[c] and Luca Rocchigiani *[a,b]

Received 28th November 2022,
Accepted 7th December 2022

DOI: 10.1039/d2dt03833a

rsc.li/dalton

Zirconocene cations react with Cp_2WH_2 affording the bimetallic $[Cp_2Zr(\mu\text{-}H)(\mu\text{–}\eta^1\text{:}\eta^5\text{-}C_5H_4)WHCp]^+$ bridging hydride **1** (Cp = cyclopentadienyl anion, $C_5H_5^-$) *via* σ-bond metathesis. Complex **1** features an atypical out of plane Zr(μ-H)W moiety, where no intermetallic interaction is involved, and a fluxional core. Coordination geometry and bond distances of the bridging hydride interaction can be modulated upon reaction with Lewis bases and unsaturated substrates. PMe_3, P(*p*-tol)$_3$, 3,5-dimethylpyridine and THF bind to **1** and shift the hydride bridge on the coordination plane of Zr. Insertion of olefins and alkynes into the Zr–C bond of **1** leads instead to alkyl and vinyl species where the Zr and W coordination planes are perpendicular to each other. Such alterations of the Zr(μ-H)W arrangement are reflected in the average ^{1}H NMR chemical shift values of the hydride, which correlate linearly with computed Zr–H distances. Reactivity experiments with H_2 showed that the bridging hydride interaction prevents bimetallic cooperativity and that σ-bond metathesis between Zr–C and H–H bonds is the preferred pathway for all the investigated complexes.

Introduction

Heterobimetallic complexes have attracted considerable interest over the past decades for their potential in triggering chemical reactivity that would not occur with a single specific transition metal or main group element.[1–3] In this respect, the combination of two fragments with complementary Lewis acid/base properties is particularly interesting, as it can lead to polarization and cleavage of small molecules bypassing the classic monometallic pathways and enable important catalytic applications.[4,5]

There are multiple ways to make two metal fragments interact with each other, which go beyond the simple formation of unsupported metal–metal bonds. One strategy is to use bridging ligands to provide additional thermodynamic stabilisation to the intermetallic bonding. Bridging hydrides are among the most widespread examples and constitute a common structural feature of many heterobimetallic complexes, ranging from cluster compounds to metalloenzymes.[6–8] Such interactions are generally described as 3-center–2-electron (3c2e) bonds[9] and show usually higher stability than their terminal M–H counterparts. Nonetheless, they may retain chemical reactivity arising from the electron deficiency at the metal centres, which makes bimetallic hydrides, for instance, good models for catalytically relevant hydrogenation[10] and hydroelementation intermediates.[11,12]

Bimetallics based on highly Lewis acidic zirconocenes of the type $Zr(\mu\text{-}H)_nTM$ or $Zr(\mu\text{-}H)_nE$ (TM = transition metal, E = main group element) form an important class of bridging hydride complexes and take part in many stoichiometric and catalytic reactions. Notable examples include cationic $[L_2Zr(\mu\text{-}H)_3(Al^iBu_2)_2][X]$ complexes (**a**, Fig. 1, L_2 = bis-cyclopentadienyl or *rac*-bridged bis-indenyl), which have been investigated by Bercaw and Brintzinger in the context of olefin polymerisation,[13–15] or the neutral $Cp_2Zr(H)(\mu\text{-}H)(N = {}^tBu)IrCp^*$ (**b**, Fig. 1) reported by Bergman as the product of cooperative H_2 activation by Zr–Ir bimetallics.[16] More recently, $Cp_2Zr(H)(\mu\text{-}H)_2Zn$(diketimine) (**c**, Fig. 1) complexes have found application in olefin isomerisation catalysis.[17,18] A peculiar combination originates when electropositive zirconocenes are combined with nucleophilic metal hydrides based on the middle-late portion of the transition series, as the two metals have complementary electronic characteristics. There are a few examples of bimetallics of such kind beyond Bergman's complex **c**, like the neutral bridging polyhydrides $Cp_2ZrCl(\mu\text{-}H)_3ML_n$ (ML_n = $Os(PMe_2Ph)_3$,[19] $IrCp^*$,[20] **d** and **e**, Fig. 1) and

[a]*School of Chemistry, University of East Anglia, Norwich Research Park, NR47TJ Norwich, UK*
[b]*Department of Chemistry, Biology and Biotechnology and CIRCC, University of Perugia, I-06123 Perugia, Italy. E-mail: luca.rocchigiani@unipg.it*
[c]*Department of Chemistry, University of Naples Federico II, Via Cintia, I-80126 Naples, Italy. E-mail: p.budzelaar@unina.it*

† Electronic supplementary information (ESI) available. CCDC 2212595–2212600. For ESI and crystallographic data in CIF or other electronic format see DOI: https://doi.org/10.1039/d2dt03833a

‡ These two authors contributed equally.

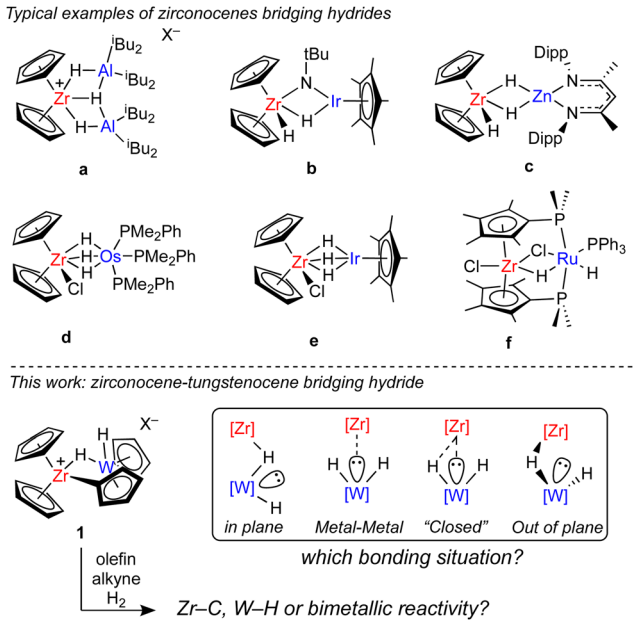

Fig. 1 Contextualisation of the present work.

$Cp_2ZrCl\{H_5W(PMe_3)_3\}$,[21] or the chloro-hydrido bridging $Cl_2Zr(Cp^*PMe_2)_2(\mu\text{-}H)Ru(H)(Cl)PPh_3$ complex (**f**, Fig. 1).[22] Despite their stability, the reactivity of these species towards small molecules remains a largely unexplored topic.

In terms of bonding, it has been proposed that some of these species may contain intermetallic interactions approaching what can be called a "closed" bridging hydride situation.[23] This would occur upon populating one empty orbital on the zirconocene with electron density from the second metal, ideally in the plane perpendicular to the $Cp_{centroid}$–Zr–$Cp_{centroid}$ plane.[24] The presence of intermetallic interactions is generally invoked to account for short metal–metal distances obtained by X-Ray diffraction analysis or to explain peculiar trends in the ^{1}H NMR chemical shift values of the hydride in solution. As these examples are quite scattered and involve different metals and ligands, unequivocal trends on the bonding situation in this family of compounds cannot be drawn.

Herein we aimed at exploring more systematically the interaction between zirconocenes and nucleophilic hydrides by using Cp_2WH_2 as a prototypical electron-rich hydride donor. Cp_2WH_2 has been successfully used as ligand for many Lewis acidic transition metals and main group elements,[25–29] owing to its strong nucleophilicity arising from the formal d^2 electron configuration at the metal. This makes such complex a potential hydride and lone pair donor, and it becomes interesting to understand how it interacts with electropositive cationic metallocenes Cp_2ZrX^+ having, in theory, two empty orbitals available for bonding. In this scenario, several arrangements may be active, ranging from typical in-plane interactions to out-of-plane bridges, passing through metal–metal stabilised structures, with or without bridging hydride (Fig. 1).

To investigate such scenarios, we used zirconocenium alkyl cations to metalate Cp_2WH_2 and synthesize the novel cationic bimetallic bridging hydride $[Cp_2Zr(\mu\text{-}H)(\mu\text{-}\eta^1{:}\eta^5\text{-}C_5H_4)WHCp]^+$ **1** (Fig. 1). The geometry of **1** is peculiar, as the metalation of one Cp ring of tungstenocene makes the bimetallic complex flexible enough to probe the selectivity for establishing a bridging hydride interaction or the metal–metal bond. Therefore, it makes a very useful platform to evaluate the tendency of zirconocene cations to accept electron density from a metal hydride. Moreover, complex **1** contains three coexisting functionalities (metal hydride, Zr–C bond and potential intermetallic interaction) and it becomes intriguing to probe its reactivity towards small molecules like alkenes, alkynes or H_2 and test what is the most reactive site. To investigate these aspects, we use NMR spectroscopy, X-Ray diffraction and DFT calculations, and we rationalize how different Zr(μ-H)W arrangements affect the spectroscopic properties and bonding in this class of complexes.

Results and discussion

σ-Bond metathesis reactions

To explore reactions between zirconocenes and tungstenocenes, $[Cp_2ZrMe^+\cdots MeB(C_6F_5)_3^-]$[30] and $[Cp_2Zr(\eta^2\text{-}CH_2\text{–}NMePh)][B(C_6F_5)_4]$[31,32] were chosen as starting materials as they can be straightforwardly prepared *in situ* from Cp_2ZrMe_2 and $B(C_6F_5)_3$ or $[HNMe_2Ph][B(C_6F_5)_4]$. These ion pairs were reacted with 1 equivalent of Cp_2WH_2 in C_6D_6/*ortho*difluorobenzene (ODFB, 10 : 1 v/v) at 297 K. ^{1}H NMR indicated that a fast and quantitative reaction takes place upon mixing the reagents, leading to the formation of the bimetallic ion pair **1X** (X^- = $MeB(C_6F_5)_3^-$, $B(C_6F_5)_4^-$), featuring the tungstenocene fragment covalently bound to the Zr centre (Fig. 2). Concurrently, the formation of CH_4 or Me_2NPh was observed. ^{13}C NMR spectroscopy indicated that the σ-metalated carbon atom is high-frequency shifted at δ_C = 152.8 for **1B(C_6F_5)$_4$** and δ_C = 153.2 ppm for **1MeB(C_6F_5)$_3$** (δ_C Cp_2WH_2 *ca.* 75.0 ppm), while the hydride signal appears as a singlet in the ^{1}H NMR spectrum for both complexes at δ_H = −11.7 ppm, with ^{183}W satellites ($^1J_{WH}$ = 76.5 Hz). Broadening of this resonance was observed upon cooling down a sample of **1B(C_6F_5)$_4$** in C_7D_8/ODFB to −70 °C, but no decoalescence was obtained. The methylborate anion in **1MeB(C_6F_5)$_3$** shows NMR fingerprints which are in between those of an inner and an outer sphere ion pair (δ_H(B–Me) = 0.82 ppm, $\Delta\delta$(*m*-F/*p*-F) = 3.5 ppm),[33] suggesting that the anion is sterically prevented from establishing a strong coordination to the Zr. Analogously, the aniline released upon the formation of **1B(C_6F_5)$_4$** does not coordinate to the metal centre.

The formation of **1MeB(C_6F_5)$_3$** was also probed at low temperature, by adding 1 equivalent of Cp_2WH_2 to a solution of $[Cp_2ZrMe^+\cdots MeB(C_6F_5)_3^-]$ in C_6D_5Cl at −50 °C. Under these conditions, the formation of the bimetallic ion pair $[Cp_2ZrMe(H_2WCp_2)][MeB(C_6F_5)_3]$ (**I**) was observed, implying that Cp_2WH_2 coordinates to the zirconocene before being σ-meta-

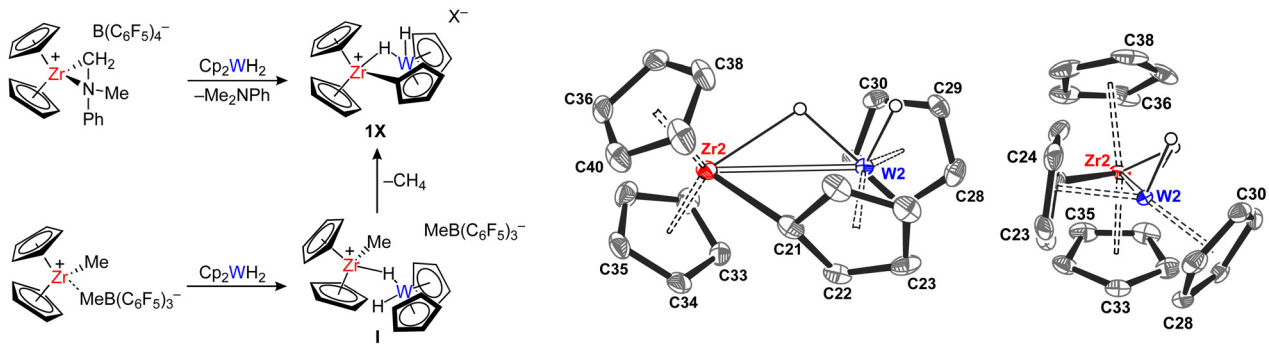

Fig. 2 Left: synthesis of **1X** (X^-=$B(C_6F_5)_4^-$ or $MeB(C_6F_5)_3^-$). Right: two views of the molecular structure of **1B(C$_6$F$_5$)$_4$** (one of the two independent molecules found in the asymmetric unit is shown). Non-hydride hydrogen atoms and anion are omitted for clarity, thermal ellipsoids are drawn at 50%. Selected distances [Å] and bond angles [°]: Zr2–W2 3.1395(6), Zr2–C21 2.268(4), $Cp_{centroid}$–Zr–$Cp_{centroid}$ 129.45, $Cp_{centroid}$–W–$Cp_{centroid}$ 144.85, Zr2–C1–$Cp_{centroid}$ 146.84.

lated. According to ^{1}H and ^{19}F NMR, **I** is an outer sphere ion pair (δ_H(BMe) = 1.34 ppm, $\Delta\delta_F$(*m*–F, *p*–F) = 2.7 ppm), where the hydride ^{1}H chemical shift is close to that of pure Cp_2WH_2 (δ_H(**I**) = −12.7, $^1J_{WH}$ = 77 Hz) and does not show any temperature dependence. Conversion of **I** into **1MeB(C$_6$F$_5$)$_3$** and CH_4 elimination occurred simultaneously over the period of 4 hours at −40 °C, most likely through a σ-bond metathesis pathway.[34]

Emerald crystals of **1B(C$_6$F$_5$)$_4$** suitable for X Ray diffraction were obtained by layering a C_6D_6/ODFB solution with light petrol ether. Two independent molecules with very similar structural parameters were found in the asymmetric unit; they showed an average Zr–W distance of 3.126 Å, which is below the sum of the van der Waals or the covalent radii of Zr and W.[35] The tungstenocene fragment is tilted towards the zirconocene, with a Zr2–C21–$Cp_{centroid}$ angle of about 147° and a W2–Zr2–C21 angle of 46° (Fig. 2). The arrangement of the hydride moieties is asymmetric, with one hydrogen atom oriented towards the zirconium at an estimated average Zr···H distance of 2.2 Å and describing a Zr–H–W angle of about 104°. The second hydride is oriented far away from the Zr atom, at over 4 Å from the metal centre. The η^1:η^5 Cp is almost perpendicular to the zirconocene fragment, with the hydride moieties oriented out of the Zr2–W2–C21 plane by 48°. Both Zr–W and Zr–H bond distances are compatible with the presence of an interaction between the two metal fragments that leads to the bending of the Zr–C21–$Cp_{centroid}$ angle, even though the coordination geometry of the bridging hydride is considerably twisted with respect to the ideal planar arrangement. The nature of this interaction was dissected by DFT calculations (see below).

The Zr(μ–η^1:η^5–Cp)M motif is well-known and there are many examples of neutral species that have been obtained, for instance, by lithiation/transmetalation of ferrocene[36] or hydride expulsion from trimetallic Zr–Ru_2 carbonyl complexes.[37] On the other hand, reactions involving cationic zirconocenes are less common. Seminal cases are the zirconation of ferrocene by σ-bond metathesis with the Zr–Me bond of [Cp_2ZrMe^+···$MeB(C_6F_5)_3^-$],[38] or the metalation of Rh indenyl by transient alkyl metallocenes generated by $AlMe_3$.[39] Even though metalation of Cp_2WH_2 was observed previously in Ir polyhydride systems by Venanzi[40] and Moore,[41,42] as well as in lanthanide complexes by Tilley and co-workers, the "tilted" bridging hydride coordination mode on **1** seems to be less common.

Unlike **1B(C$_6$F$_5$)$_4$**, **1MeB(C$_6$F$_5$)$_3$** is not thermally stable in C_6D_6/ODFB and transforms into the orange zwitterion **2** upon CH_4 elimination over the course of 2 weeks at 297 K (Fig. 3). This is corroborated by the loss of one hydrogen from the C_5H_5 ligand bound to tungsten and a moderate high-frequency shift of the hydride signal (δ_H = −9.7 ppm, $^1J_{WH}$ = 76.5 Hz) in the ^{1}H NMR spectrum. ^{19}F NMR shows the appearance of a new set of signals for the pentafluorophenyl rings, characterised by a very broad resonance for the *ortho*-F at δ_F = −136.6 ppm suggesting the presence of Zr···F interactions.[43] The chemical shift of the σ-metalated carbon atom is slightly high-frequency shifted with respect to **1MeB(C$_6$F$_5$)$_3$** (δ_C = 160.2 *vs.* 152.8 ppm). The molecular structure (Fig. 3) is compatible with NMR observations and shows that $B(C_6F_5)_3$ attacked the second cyclopentadienyl ligand bound to tungsten. Consistently, one of the *ortho*-fluorine atoms in **2** shows a close interaction with the Zr centre ($d_{Zr–F32}$ = 2.562 Å). Despite the presence of this additional interaction at the Zr, the asymmetric hydride arrangement of the metalated tungstenocene remains unaltered with respect to **1**, with a Zr–W distance of 3.104 Å. The roughly estimated Zr···H distance of 2.38 Å is slightly longer than that in **1** and the Zr–H–W angle is 100°, just 4° lower than that observed in **1**.

The transformation of **1MeB(C$_6$F$_5$)$_3$** into **2** resembles previous reactivity reported by Braunschweig, who showed that $B(C_6F_5)_3$ reacts with Cp_2WH_2 leading to a W(VI) zwitterion of the type [{$C_5H_4B^-(C_6F_5)_3$}$CpWH_3^+$].[44] In our case, it can be speculated that transient concentrations of $B(C_6F_5)_3$ are generated upon anion coordination at the Zr and breakage of the B–Me bond, in analogy to what is often observed for zirconocene methylborate ion pairs.[30] The formed borane would then attack the W–Cp unit, form a C–B bond and release a proton, which would eventually lead to CH_4 elimination from the Zr–Me group generated upon loss of borane. Alternatively, σ-bond

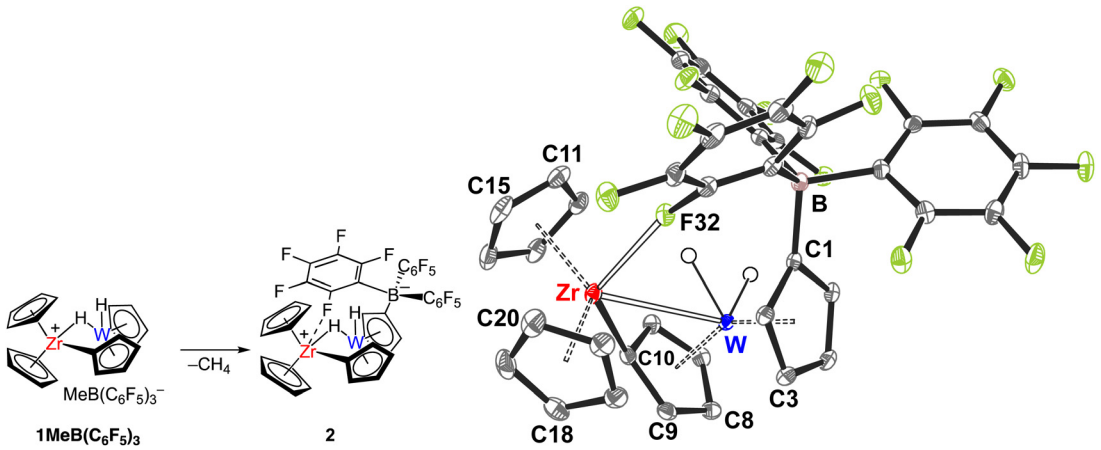

Fig. 3 Left: conversion of **1MeB(C$_6$F$_5$)$_3$** into **2**. Right: molecular structure of **2**. Non-hydride hydrogen atoms and solvent molecules are omitted for clarity, thermal ellipsoids are drawn at 50%. Selected distances [Å] and bond angles [°]: Zr–W 3.1044(6), Zr–C10 2.248(18), B–C1 1.662(3), Zr–F32 2.5626(10), $Cp_{centroid}$–Zr–$Cp_{centroid}$ 128.02, $Cp_{centroid}$–W–$Cp_{centroid}$ 147.08, Zr1–C10–$Cp_{centroid}$ 147.91.

metathesis between Zr–C and Me–B bonds could take place, leading to the formation of a borane-functionalized tungstenocene, which would eliminate CH_4 upon rotation/remetalation.

Such reactivity was not observed when the solvent was C_6D_5Cl. In the latter medium, **1MeB(C$_6$F$_5$)$_3$** showed indeed to be stable over a week at 297 K. Strikingly, freshly prepared samples of **1X** in C_6D_6 or C_6D_6/ODFB change colour from bright green to orange upon drying and redissolving in C_6D_5Cl. The same is observed when **1MeB(C$_6$F$_5$)$_3$** is synthesised *in situ* using C_6D_5Cl as solvent. The hydride signal is unaffected by the change of medium (δ_H = −11.8 ppm, $^1J_{WH}$ = 76.5 Hz), while the metalated carbon atom is slightly low frequency shifted at δ_C = 144.0 ppm with respect to C_6D_6 solutions (δ_C *ca.* 153.0 ppm). It is reasonable to assume that C_6D_5Cl coordinates strongly at the Zr centre,[45] pushing the $MeB(C_6F_5)_3^-$ anion in the second coordination sphere and preventing its degradation. Most likely, the electronic properties, hence the colour, of the bimetallic complex are affected by the solvent coordination as well. Anyway, as the spectroscopic fingerprints of the bimetallic core are basically unaltered, it can be assumed that C_6D_5Cl coordination does not disrupt the interaction between the two metal fragments.

Reactions with Lewis bases

The presumed ability of chlorobenzene to coordinate at the Zr centre of complex **1** confirms that the latter is not "saturated" by the Zr···H–W interaction and a coordinative vacancy is available for further reactivity. The lack of appreciable coordination of the $MeB(C_6F_5)_3^-$ anion (or Me_2NPh) mentioned above may be simply due to a mismatch in basicity or sterics. To probe whether using stronger or less encumbered Lewis bases leads to a different outcome, we investigated the reactions between **1MeB(C$_6$F$_5$)$_3$** and prototypical Lewis bases, such as PR_3 (R = Me, *p*-tolyl), 3,5-lutidine (3,5-dimethylpyridine) and THF.[46]

Unlike NMe_2Ph, PMe_3 reacts instantaneously with **1** and affords a mixture of two isomers in a 85 : 15 molar ratio: a *W-outside* complex (**3a**), where PMe_3 is coordinated close to the metalated Cp, and a *W-inside* complex (**3b**), where PMe_3 binds close to the bridging hydride (Scheme 1). The coordination of PMe_3 induces a considerable low-frequency shift of the hydride signal (δ_H(**1**) = −11.7 ppm), which appears at δ_H = −17.9 and δ_H = −14.3 ppm for **3a** and **3b**, respectively. Splitting of the hydride signals due to coupling with ^{31}P is observed, with J_{PH} values of 6.4 Hz for **3a** and 10.7 Hz for **3b**. The $^1J_{WH}$ values for the two isomers are appreciably different: while $^1J_{WH}$ for **3b** is very similar to that of **1** (72.0 Hz), the hydride-tungsten coupling is reduced somewhat in **3a** ($^1J_{WH}$ = 66.0 Hz). Based on these spectroscopic fingerprints, it can be inferred that the bridging hydride interaction is maintained in **3**. As in the previous case, the two hydride moieties appear as a singlet in the ^{1}H NMR spectrum, likely due to the fast averaging of chemical shift and coupling constant values over the two hydride environments (see DFT calculations).

The crystal structure of **3a** (Fig. 4) is consistent with the NMR data and shows that the planes described by the two Cp–M–Cp units are almost perpendicular, with a Zr–W distance of around 3.4 Å and a Zr–C1–$Cp_{centroid}$ angle of 154°. The Zr–P distance of 2.71 Å is unexceptional and lies in the typical range observed for Cp_2Zr–PMe_3 fragments.[47–49] The observation of a longer Zr–W distance in **3a** compared to **1** (δd_{Zr-W} = 0.3 Å) suggests that metal–metal interactions play a negligible

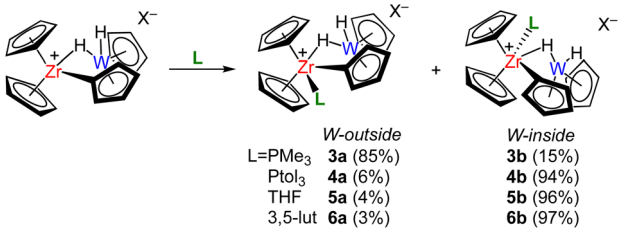

Scheme 1 Reactions of **1MeB(C$_6$F$_5$)$_3$** with Lewis bases.

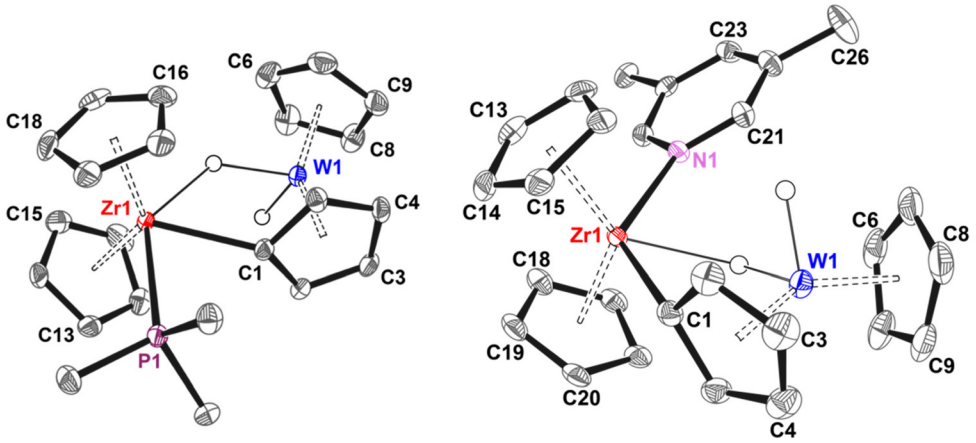

Fig. 4 Molecular structures **3a** (left, one of the two independent molecules found in the asymmetric unit) and **6b** (right). Non-hydride hydrogen atoms and anion are omitted for clarity, thermal ellipsoids are drawn at 50%. Selected distances [Å] and bond angles [°], **3a**: Zr1–P1 2.7088(8), Zr1–C1 2.316(4), Zr1–C1–$Cp_{centroid}$ 154.72, $Cp_{centroid}$–W1–$Cp_{centroid}$ 147.03, $Cp_{centroid}$–Zr1–$Cp_{centroid}$ 129.68; **6b**: Zr1–N1 2.441(2), Zr1–C1 2.307(2), Zr1–C1–$Cp_{centroid}$ 153.87, $Cp_{centroid}$–W1–$Cp_{centroid}$ 145.86, $Cp_{centroid}$–Zr1–$Cp_{centroid}$ 128.49.

role in its bonding (see DFT section). Consistently, electron density corresponding to a bridging hydride was located in the Zr coordination plane, at an approximate distance of 2.0 Å from Zr and 1.7 Å from W, establishing a Zr–H–W angle of about 130° (average between the two independent molecules in the cell). Clearly, increasing the coordination number at the Zr centre affects the geometry of the bridging hydride, which is now oriented in the same plane as the other two ligands bound to Zr.

The low abundance of **3b** makes its complete NMR assignment more difficult. In any case, the presence of a strong phosphorous-hydride coupling (stronger than **3a**) led us to formulate **3b** as a bridging hydride as well. This hypothesis is also backed by DFT calculations (see below).

The bulkier tris-*p*-tolyl-phosphine binds **1MeB(C_6F_5)$_3$** as well, but the regiochemical outcome of the reaction is reversed with respect to PMe_3. In fact, almost exclusive formation of the *W-inside* isomer **4b** (**4a** : **4b** = 6 : 94) was observed. The latter shows a dihydride signal at δ_H = −14.8 ppm ($^2J_{PH}$ = 11.3, $^1J_{WH}$ = 69.0 Hz) and a ^{31}P NMR signal located at δ_P = 18.2 ppm. The stereochemistry of **4b** was elucidated by NOE experiments, which revealed the presence of strong dipolar contacts between the aromatic protons of $Ptol_3$ and the hydride moieties. Consistently, no interactions were observed between tolyl rings and the σ-metalated Cp ring.

Remarkably, the ^{1}H and ^{13}C NMR spectra of **4b** show the presence of two different sets of signals for the *p*-tolyl rings in a 2 : 1 ratio, suggesting that the rotation of the phosphine about the Zr–P bond is slow (or frozen) on the NMR timescale. Most reasonably, two tolyl rings are oriented towards the zirconocene, while the other is pointing towards the tungstenocene, making them magnetically not equivalent (see ESI†). As only 2 sets of *ortho* and *meta* C–H groups are observed in total, a fast process interconverting **4b** into its mirror image must be active. Most likely, the fast hydride interconversion process averaging the two W–H chemical shifts is also responsible for such an effect.

In contrast with **3a–b**, ^{1}H NOE NMR also indicates that **4a** and **4b** are in chemical exchange. For example, intense exchange cross peaks were observed between the hydrides of **4a** and **4b** or between the W–Cp rings of the two isomers. Reasonably, **4a** and **4b** form a thermodynamic mixture equilibrating through phosphine dissociation/migration. In agreement with the latter hypothesis, the addition of a second equivalent of $Ptol_3$ to the mixture enables chemical exchange between coordinated and free phosphine, corroborating the presence of a labile Zr–P bond in **4** (ESI†).

Preference for *W-inside* coordination was also observed with THF and 3,5-lutidine (selectivity >95%). In the case of the former, the hydride signal of the *inside* adduct **5b** is considerably broad at room temperature (δ_H = −13.8 ppm), while it sharpens into a well-defined singlet with ^{183}W satellites ($^1J_{WH}$ = 73 Hz) when the sample is cooled down to 253 K. By using ^{1}H NOE NMR at this temperature it is possible to detect chemical exchange between **5a** and **5b**, as observed in the case of $Ptol_3$, confirming that binding of THF to Zr is loose. Moreover, if a small excess of THF (1.33 mol) is used, free and coordinated THF signals are averaged at room temperature and can be separated only at 253 K. This indicates that broadening of the W–H signals is due to THF fluxional coordination, rather than internal hydride dynamicity. The identity of **5b** was confirmed by ^{1}H NOESY, which revealed selective interactions between the hydride signals and α- and β-THF protons, while the latter do not interact with the σ-metalated Cp. As in the previous cases, the relative concentration of **5a** was too low for a compelling NMR assignment.

3,5-Lutidine reacts with **1MeB(C_6F_5)$_3$** forming the stable adduct **6b** in 97% selectivity. Contrary to the results obtained with THF, the hydride resonance appears as a sharp singlet located at δ_H = −14.4 ppm, with $^1J_{WH}$ = 73 Hz. ^{1}H NOESY NMR

showed dipolar contacts between the pyridine protons and the hydride signal, while there is no interaction with the σ-metalated tungsten-cyclopentadienyl, as observed for **5b**. Moreover, chemical exchange between *inside* and *outside* isomers was observed, implying labile coordination of nitrogen as in the cases of THF and $Ptol_3$. The solid-state molecular structure of **6b** (Fig. 4) is in perfect agreement with the NMR data, showing that the coordination of 3,5 lutidine occurs in proximity of the hydride moieties and opposite to the σ-metalated cyclopentadienyl. The Zr1–N1 distance of 2.441(2) Å is in line with other previously reported zirconocenium pyridine adducts[50] and the Zr1–C1–$Cp_{centroid}$ angle of 154° matches that of complex **3a**. Electron density compatible with the presence of a bridging hydride was located at an approximate Zr···H distance of 2.1 Å showing a Zr–H–W angle of 123°, which is slightly lower than that observed in **3a**.

The picture emerging from the reactivity of **1MeB(C_6F_5)$_3$** with Lewis bases is that the Zr centre of the bimetallic complex can accommodate ligands with sufficient basicity and different steric demand, originating adducts with a regiochemistry that depends on the nature of the base. Irrespective of the *W-inside* or *W-outside* configuration, the geometry of the bimetallic core is considerably affected by the coordination of the base with respect to **1** and the clear formation of *in-plane* bridging hydride interaction is observed. In the case of the **4**, **5** and **6**, the coordination of the base is labile and exchange between the two regioisomers occurs. On the other hand, with the PMe_3 complex **3** such exchange does not take place (or is too slow to be observed by NMR), most likely owing to its higher Lewis basicity.

Insertion reactions

The presence of an accessible coordinative vacancy in *cis* position to the σ-metalated Cp opens to the possibility to exploit insertion of double and triple bonds into the Zr–C bond to tweak the interaction between Zr and the W–H bonds.

1MeB(C_6F_5)$_3$ reacts with internal alkynes affording products whose structure depends on the substituents on the triple bond. Electron rich alkynes, such as 2-butyne, insert exclusively into the Zr–C bond leading to the corresponding *cis*-vinyl-cyclopentadienyl products **7** (Fig. 5). In the case of asymmetric substrates (R ≠ R′), mixtures of insertion products are observed. Generally, the bulkiest group is preferentially inserted close to the Cp bound to tungsten: with 1-phenyl propyne, a molar ratio of 70 : 30 was observed while this increased to 80 : 20 when 4,4′dimethyl-2-pentyne was used. In the latter case, the mixture evolves to 100% of the 2,3 insertion products over the course of 48 h, suggesting that a kinetic mixture was initially obtained. The interconversion between the two isomers is likely to occur through a β-carbon elimination–reinsertion sequence, which is not unprecedented in zirconocene alkyne chemistry.[51] In the case of the bulky bis-adamantyl acetylene, no insertion was observed over the period of 7 days at room temperature.

Alkyne insertion products **7a–c** display a high-frequency shift of the hydride resonance of about 2 ppm with respect to **1** and a moderate increase of the $^1J_{WH}$ values to around 80 Hz. This is consistent with a further alteration in the interaction mode between the Zr centre and the WH_2 moiety. The molecular structure of **7c** (Fig. 5), obtained by X-Ray diffraction, shows that the orientation of the two metallocene fragments is almost perpendicular, with the whole Zr–vinyl–tungsten unit lying in the same plane and the two W–H groups oriented above and below this plane. Despite the different orientation, the W–Zr distance is only marginally shorter than that in **1** (3.087 Å), suggesting the presence of an interaction between the two fragments that is not much stronger than that of the starting complex. However, the coordinative vacancy in these insertion products is less accessible with respect to **1**. For

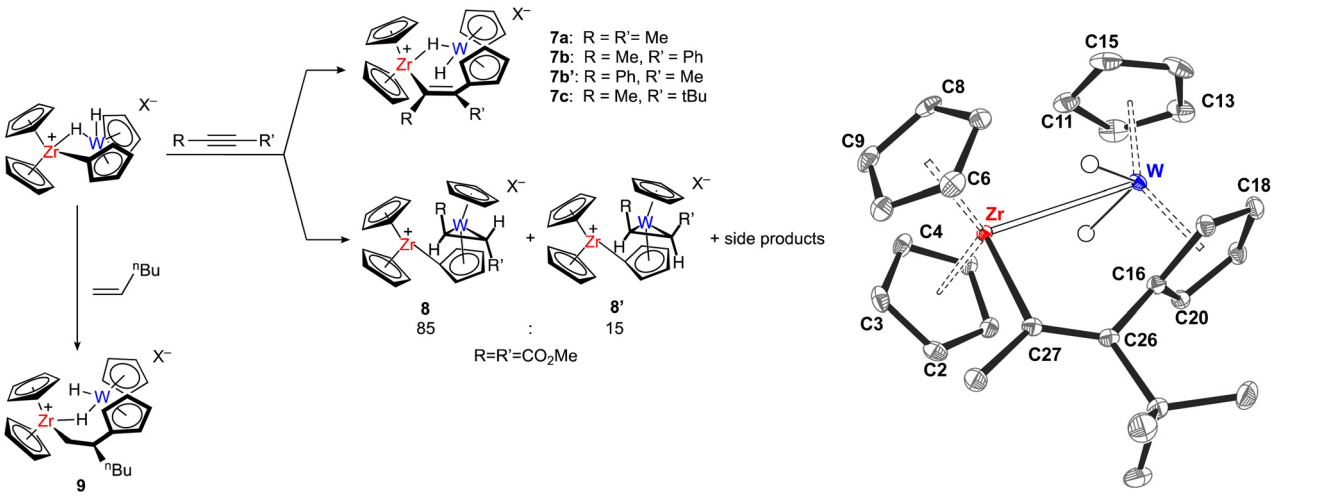

Fig. 5 Left: reactivity between **1** and alkynes/alkenes. Right: molecular structure **7c**. Non-hydride hydrogen atoms and $MeB(C_6F_5)_3^-$ anion are omitted for clarity, thermal ellipsoids are drawn at 50%. Selected distances [Å] and bond angles [°]: Zr–W 3.0878(2), Zr–C27 2.268(2), C26–C27 1.349(3), $Cp_{centroid}$–Zr–$Cp_{centroid}$ 126.21, $Cp_{centroid}$–W–$Cp_{centroid}$ 144.42, C26–C16–$Cp_{centroid}$ 164.60.

example, **7c** does not react with excess PMe_3 and the ^{31}P NMR signal of free phosphine can be detected in solution for at least 24 h at room temperature. After a few days, slow decomposition processes to unidentified species took place.

Using electron-poor alkynes, such as dimethyl-acetylenedicarboxylate (DMAD), flips the reactivity and insertion occurs into the W–H bond. The outcome of the reaction is composed of a complex mixture of isomeric bimetallic complexes where no W–H signals are detected by ^1H NMR. Such a complex mixture evolves over the course of 1 week, generating two main sets of signals in 85 : 15 ratio, with a spectroscopic yield of about 60%. The ^1H NMR spectrum of the major product showed the presence of two magnetically inequivalent doublets ($^3J_{HH}$ = 10.8 Hz) at δ_H = 1.67 and δ_H = 3.33 ppm, together with two –OMe singlets (δ_H = 3.31 and δ_H = 3.54 ppm), showing long-range correlations with two signals at δ_C = 7.7 and δ_H = 8.6 ppm in the ^{13}C NMR spectrum. This pattern is consistent with a double insertion of one DMAD molecule into both the W–H bonds of **1MeB(C_6F_5)$_3$**, which leads to the formation of tungstenocycle **8**, in analogy to what previously observed by Herberich and Barlage on Cp_2WH_2.[52] The stereochemistry of **8** was determined by using ^1H NOE experiments, which revealed the presence of a dipolar interaction between the C–H group of the metallacyclopropane at δ_H = 1.67 ppm and a W–Cp singlet at δ_H = 4.40 ppm. On the other hand, the second C–H group (at δ_H = 3.33) interacted with the Zr–Cp oriented towards the opposite direction, thus confirming the mutual *trans* arrangement of the two C–H groups. According to ^{13}C NMR, the η^1:η^5 Cp ring remains intact, with its quaternary carbon atom resonating at δ_C = 142.0 ppm, in analogy to **1**. The second set of signals was attributed to the *cis* isomer **8′**, again based on ^1H NOE interactions. Unfortunately, no single crystals of **8** or **8′** could be obtained and the nature of the interactions between the two metal centres could not be ascertained.

1MeB(C_6F_5)$_3$ reacts also with 1-hexene, undergoing 1,2 insertion into the Zr–C bond and affording the corresponding bimetallic alkyl-bridged derivative **9** (Fig. 5). Even when a large excess of olefin was used, no trace of polymerisation was observed at room temperature. Complex **9** shows a Zr–CH_2 moiety at δ_C = 53.7 ppm bearing two magnetically inequivalent hydrogen atoms located at δ_H = 1.44 and δ_H = −0.44 ppm in the ^1H NMR spectrum. Interestingly, the two hydrides were also found to generate two different signals δ_H = −10.7 and δ_H = −10.8 ppm, coupled with each other with a $^2J_{HH}$ = 6.3 Hz. Most likely, this splitting is due to the diastereotopic character of the two hydride moieties. These two signals show two different satellite couplings with ^{183}W of 83.2 (H *anti* to the butyl chain) and 76.4 Hz (H *syn* to the butyl chain), implying that the degree interaction between the two hydrides and the Zr centre is not symmetric, as proposed for all the other complexes above.

Reactions with H_2

We previously reported that zirconaziridinium salts react with H_2 undergoing hydrogenolysis of the Zr–CH_2 bond leading to an intermediate zirconocene hydride amine complex that splits H_2 heterolytically.[53] Complexes **1X** can be seen as analogues of zirconaziridium ion pairs, in which the σ-metalated Cp and the tungsten atom replace the CH_2–NR_2 group. In this respect, it is interesting to test whether hydrogenolysis leads to the same outcome or the presence of the tungsten centre enables other reaction pathways. In addition, it is also of interest to probe how the different structures that have been derived from **1** upon reaction with bases or alkynes/alkenes affect H_2 activation.

1B(C_6F_5)$_4$ reacts slowly with H_2 (298 K, 1 atm), producing initially a ^1H NMR spectrum with broad resonances that evolves to two major sets of signals over the course of 2 days. The first was assigned to $[Cp_2WH_3][B(C_6F_5)_4]$, based on the appearance of the typical pattern of W(VI) trihydrides with a doublet at δ_H = −7.13 ppm and a triplet located at δ_H = −6.55 ppm ($^2J_{HH}$ = 9.6 Hz).[54] The second set of signals was assigned to the trimetallic complex **10**, containing a hydride bridged zirconocene dimer bearing a doubly σ-metalated tungstenocene dihydride facing the two Zr centres (Fig. 6). Complex **10** showed two different hydride resonances in the ^1H NMR: a broad triplet, without ^{183}W coupling, resonating at δ_H = −5.50 ppm and a sharp doublet with ^{183}W satellites ($^1J_{WH}$ = 70.5 Hz) at δ_H = −12.7 ppm. Single crystals of complex **10** were obtained from double layering a concentrated C_6D_5Cl solution with light petrol ether. The corresponding molecular structure revealed that the metalated tungstenocene orients the hydrides towards the coordinative vacancies of both the Zr centres, at tungsten–zirconium distances of 3.413 Å (W1–Zr2) and 3.313 Å (W1–Zr3). The Zr2–Zr3 distance is 3.762 Å and the estimated Zr···H distances are comprised between 2.5 and 2.9 Å. While the intrinsic uncertainty in the estimation of H positions does not allow to precisely understand the nature of the Zr···H bonding, the presence of a 2.7 Hz coupling between Zr–H and W–H signals implies the presence of a residual interaction between them.

From a mechanistic standpoint, the formation of **10** requires two extra H atoms, hence splitting of one H_2 molecule. Even though an hydridic Zr(μ-H) and a protic W(VI) hydride are formed, it is likely that this reactivity is not due to heterolytic hydrogen splitting at the bimetallic core. More reasonably, an hydrogenolysis route analogous to that of zirconaziridium salts takes place. In this scenario, coordination of H_2 to the Zr of **1** would enable σ-bond metathesis between the H–H and the Zr–C bonds, leading to the regeneration of Cp_2WH_2 and formation of a zirconocenium hydride. The latter could react quickly with residual **1** establishing a bridging interaction and forming an intermediate that would undergo deprotonation by transient Cp_2WH_2 to give **10** and $Cp_2WH_3^+$. Complex **10** seems to be a thermodynamic sink, as it does not react further in the presence of excess H_2, at least for 2 weeks at RT.

Consistently, saturated complexes are much less reactive with H_2 than **1**. In the case of complex **6b**, traces of **10** formed, together with the formation of $Cp_2WH_3^+$ and Cp_2WH_2, suggesting that hydrogenolysis takes place also for this com-

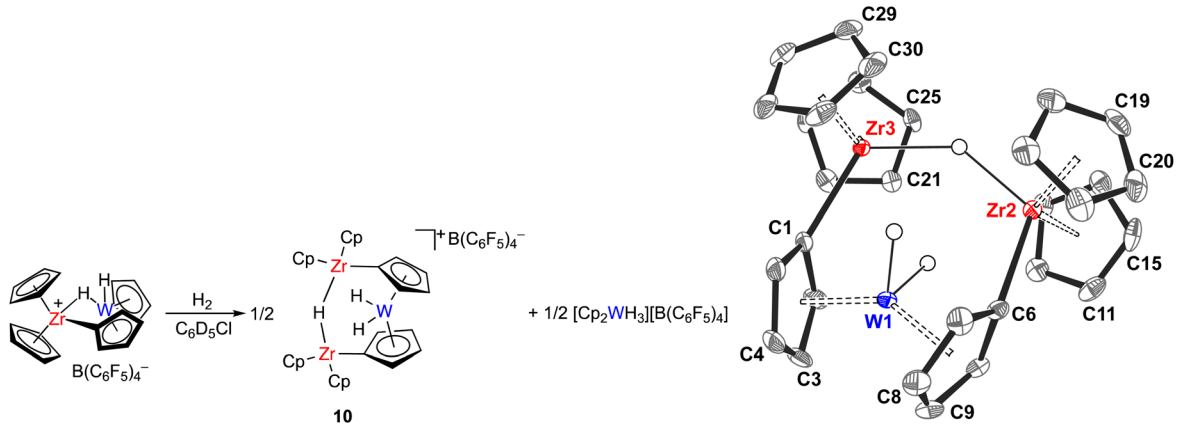

Fig. 6 Left: reaction of **1B(C$_6$F$_5$)$_4$** with H$_2$. Right: molecular structure of **10**, non-hydride H atoms and anion are omitted for clarity, thermal ellipsoid are shown at 50% probability. Selected distances [Å] and bond angles [°]: Zr3–C1 2.263(3), Zr2–C6 2.260(4), Cp$_{centroid}$–W1–Cp$_{centroid}$ 141.05.

pound. However, only a 15% conversion was observed after 7 days at RT. Complexes **3a–b** were also found to be rather unreactive and only minor side reactivity was observed after 2 weeks at RT.

On the other hand, quantitative reactivity with H$_2$ was observed for the 1-hexene insertion product **9**. After 9 days at RT, the signals of the starting complex disappeared from the ^{1}H NMR spectrum to afford a mixture of products with rather similar spectroscopic fingerprints to those obtained for the reaction of **1**. Several hydride signals were observed at δ_H = −5.34 to −5.37 ppm (Zr μ-H), δ_H = −11.79, −11.81, −12.50, −13.12, −13.15 ppm (W^{IV}–H) and δ_H = −6.04, −6.36, −6.70 (W^{VI}–H), whose presence suggests that a hydrogenolysis–deprotonation sequence may be active also for complex **9**. 2D NMR methods allowed the formed W(VI) species to be assigned as the cationic hydride **12**, featuring a 1-methylpentyl substituent on one Cp ring. The presence of a stereocenter makes the three hydride moieties in **12** magnetically inequivalent, so they appear as three distinct pseudotriplets with $^2J_{HH}$ values of 8.2 and 8.7 Hz and typical $^1J_{WH}$ of 47.4 and 68.7 Hz. While their complete NMR assignment is hampered by extensive overlapping, the two main Zr-containing products can be formulated as the isomeric trimetallic complexes **11a–b**, in which the substituted Cp ring is metalated either in α or β position with respect to the 1-methylpentyl substituent. Complexes **11** show strong dipolar contact between the W–H signals, which are magnetically inequivalent, and the Zr μ-H ones. Moreover, NOE interactions between the Zr–Cp rings and the aliphatic signals of the alkyl chain were observed. Quaternary carbon signals compatible with σ-metalated Cp were identified at δ_C = 140.0 and δ_C = 139.8 ppm in the ^{13}C{^{1}H} NMR spectrum (ESI†).

The formation of 1-methylpentyl chains from **9** indicates that σ-bond metathesis between the Zr–CH$_2$ moiety and H$_2$ most likely takes place, forming Zr–H moieties and Cp(1-methylpentyl-Cp)WH$_2$. At this stage, it is possible that the functionalised tungstenocene is remetalated at either the C$_5$H$_5$ or the C$_5$H$_4$R ring producing an intermediate that resembles **1**. The latter would undergo the same reactivity with H$_2$ described above, where the W(IV) dihydride acts as a base and is protonated upon a second Cp metalation, affording **11** and **12**. In any case, reactivity is less straightforward than that of **1**, and the trimetallic complexes are obtained in approximately 30% spectroscopic yield (Scheme 2).

The reactivity with H$_2$ of the alkyne insertion product **7c** is even more complex. After 3 weeks at RT, the signals of the starting complex disappeared from the ^{1}H NMR spectrum to originate a plethora of species. In the hydridic region of the spectrum, two main tungsten species were observed along with other secondary products showing chemical shift values similar to that of **11a–b** (δ_H = −5.33, −5.55, −11.27, −12.60 and −13.12 ppm). 1D and 2D NMR experiments allowed to assign the two tungsten species to W(VI) cyclopentadienyl-vinyl and alkyl trihydrides, which formed in 37% and 18% respectively (ESI†). The formation of the latter suggests that, as in the case

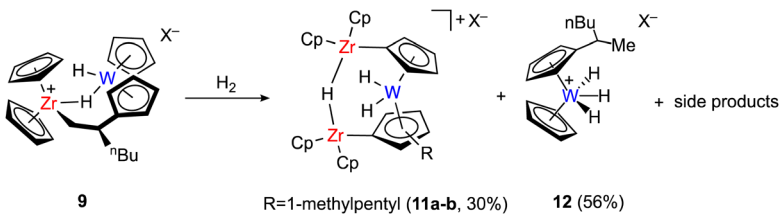

Scheme 2 Hydrogenolysis of complex **9**.

of **1**, Zr–C hydrogenolysis takes place. However, the increased steric demand of **7c** prevents the efficient trapping of transient Zr–H into bridging species and the formation of trimetallic species occurs only in traces. As previously reported by Jordan and co-workers, cationic zirconocene hydrides react in chlorobenzene under ambient light to give mixtures of dimeric bridging hydrides and chlorides.[55] It is likely that the formation of such species triggers further collateral reaction with H_2 and tungstenocene species. The formation of **11**, where a fully hydrogenated alkyl chain is present, may be related to a reinsertion–hydrogenolysis of **10** into one of the transient Zr–H mentioned above.

DFT calculations

Density functional calculations were performed to shed some light on the formation and potential dynamic behaviour of **1**, and to explain the bonding in these bimetallic complexes. First, formation of complex **1** *via* σ-bond metathesis of **I** or its hydride analogue seems plausible from the energetic point of view, and it is found to occur *via* the typical 4-membered transition state, whose energy depends on the group that is eliminated from Zr (Me or H), see Fig. 7.

Then, we find that the Zr/W core of **1** is extremely flexible. The preferred arrangement is highly asymmetric, with two clearly inequivalent W-bound hydrides as experimentally observed in the solid state. The Cp_2Zr fragment is located outside the WH_2 wedge and interacts with only one of the two hydrides (Fig. 8a). However, a more symmetric structure is accessible that has Zr sitting inside the WH_2 wedge, still interacting mostly with one of the two hydrides (Fig. 8c). Connecting this structure with its mirror image is the C_s-symmetric inversion transition state (Fig. 8d). The whole *asym–sym–asym* sequence is calculated to happen within a band of <2 kcal mol^{-1}, explaining the effective equivalence of the two hydrides as observed by NMR.

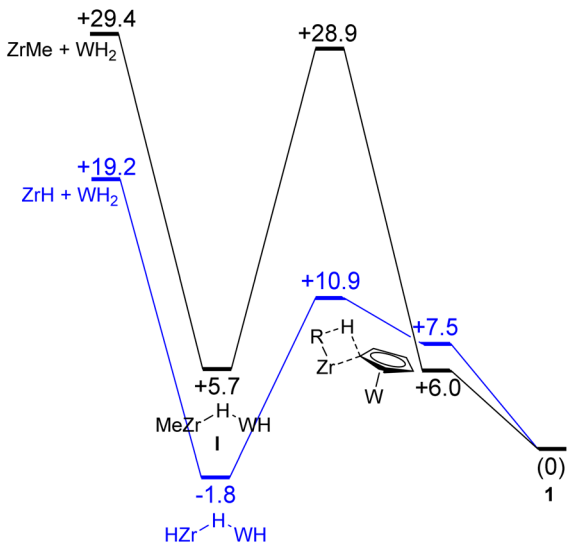

Fig. 7 Energy profile for formation of **1**.

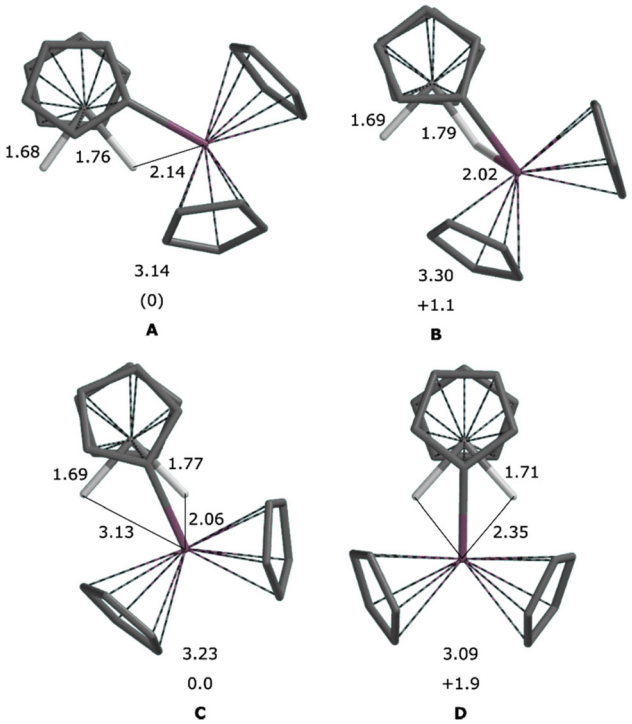

Fig. 8 (A) Asymmetric calculated "out" structure of **1**; (B) TS for in–out rearrangement; (C) "in" local minimum, and (D) C_s-symmetric inversion TS, with Zr–W bond lengths. Distances in Å. Relative free energies in kcal mol^{-1}. Cp H atoms omitted for clarity.

Structures of Lewis base (PMe_3, $PTol_3$, THF, 3,5-lut) adducts were also optimised using DFT, which confirmed the existence of separate *outside* and *inside* local minima (see Fig. 9 for **3a**/**b**). In agreement with experimental observations, PMe_3 has the largest binding energy (see Table 1) and is also the only base to prefer the *outside* arrangement. The calculated binding energies for **4–6** are compatible with fluxional behaviour (reversible base dissociation) although the stability of **4b** is probably overestimated at the computational level employed.

The nature of the interaction between the two metallocene fragments of **1** is not immediately obvious. In a seminal 1976

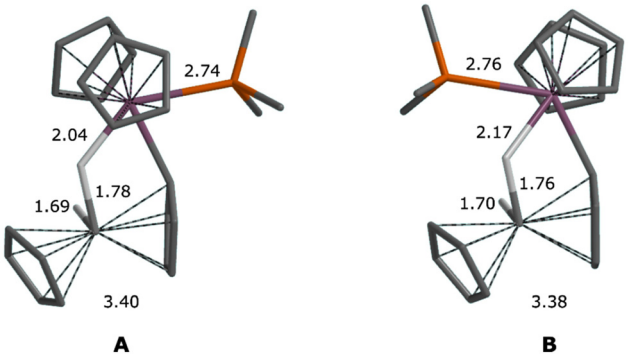

Fig. 9 Calculated structures of (A) **3a** and (B) **3b**, with Zr–W bond lengths. Distances in Å. Non-hydride H atoms omitted for clarity.

Table 1 Calculated Lewis base binding free energies (kcal mol^{-1})

	Outside	Inside
PMe_3 (**3**)	−18.7	−17.9
$Ptol_3$ (**4**)	−11.7	−17.0
THF (**5**)	−6.3	−8.5
3,5-lut (**6**)	−12.4	−15.2

paper, Lauher and Hoffmann[24] analysed the bonding capabilities of bent-metallocene fragments. They concluded that such fragments have available for bonding three valence orbitals lying in the coordination plane between the two Cp rings. In Cp_2WH_2, two of them are used to form the W–H bonds. The third contains a metal-centered lone pair (LP) and can be protonated to form the well-known $Cp_2WH_3^+$ cation. In the same way, Cp_2WH_2 could react with Lewis acids to form metal–metal dative bonds.[56–58] Alternatively, the W–H bonds could act as donors to form one or two 3c2e bonds. Recent computational work suggests that the latter bonding mode is preferred.[59,60] (Cp_2MoH_2 has also been found to form metal complexes,[29,60–63] for which similar bonding options are conceivable). We have used IBOview (IBO: Intrinsic Bond Orbital)[64,65] to analyse the situation; Fig. 10 shows relevant orbital plots, and Table 2 shows the numbers of electrons from W, H and Zr contributing to the most relevant IBOs. Shown in the figure are the W–H bonding IBO (Fig. 10A and B) as well as the lone pair (10C) of Cp_2WH_2. It can be seen immediately that the LP has most of its density away from the mouth of the wedge and is not ideal for mixing with the Zr fragment.

Fig. 10D–F show the corresponding IBOs for the asymmetric ("out") structure of **1**. The W lone pair (10F) has negligible mixing in of Zr, while one W–H bonding IBO mixes with 0.107 e of Zr, conferring some 3c2e character on this bond. On rearrangement to the C_s symmetric inversion TS, the Zr mixing is spread out over the two W–H bonds (0.066 and 0.072 e), but the W lone pair (Fig. 10I) remains mostly undisturbed.

Alkyne insertion into the Zr–C bond was also probed using DFT (see Fig. 11). Insertion of the parent alkyne ethyne is barrierless and highly exergonic (−31.2 kcal mol^{-1}, see Table 3). In all other cases the reaction proceeds from the separated reactants directly to the insertion TS, without an intermediate π-complex. Addition of 2-butyne has a significant barrier (13.4 kcal mol^{-1}) and is sufficiently exergonic (−20 kcal mol^{-1}) that the reverse reaction is not accessible at or around room temperature; the same holds for phenylpropyne. For the more hindered alkynes 4,4-dimethyl-2-pentyne and adamantylpropyne, initial insertion is not very regioselective, but reaction to the non-thermodynamically-preferred product (bulky group close to Zr) is only ~6 kcal mol^{-1} exergonic, making the insertion effectively (slowly) reversible.

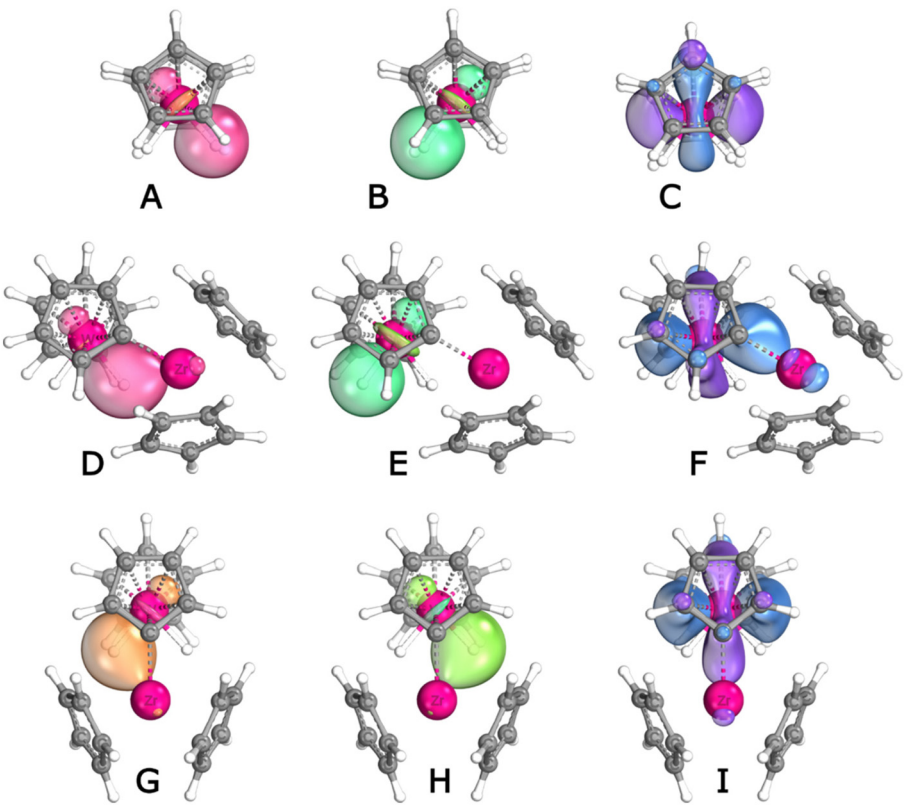

Fig. 10 (A–C) IBO for Cp_2WH_2, W–H bonds and lone pair; (D–F) IBO for the asymmetric ("out") structure of **1**: 3c2e bond, W–H bond and lone pair; (G–I) IBO for symmetric inversion TS of **1**, W–H bonds and lone pair.

Table 2 Compositions (in e) of IBOs for W LP and W–H bonds[a]

IBO:	W LP		W–H			W–H–Zr		
contr. from:	W	Zr	W	H	Zr	W	H	Zr
Cp_2WH_2	1.546	—	0.733	1.175	—	0.733	1.175	
$Cp_2ZrH\cdots H\cdots WCp_2$	1.588	—	0.729	1.167	—	0.476	1.332	0.106
1, *out*	1.639	—	0.811	1.108	—	0.464	1.341	0.107
1, *ioTS*	1.624	—	0.746	1.157	—	0.386	1.416	0.115
1, *in*	1.613	—	0.712	1.179	—	0.426	1.382	0.110
1, *ii'TS*[b]	1.635	—	0.591	1.248	0.066	0.574	1.261	0.072
3a	1.596	—	0.727	1.175	—	0.422	1.368	0.104
3b	1.600	—	0.684	1.203	—	0.472	1.334	0.082
7a[b]	1.609	0.046	0.674	1.181	0.059	0.612	1.220	0.079

[a] Contributions larger than 0.02 e. [b] Zr interacts with both hydrides.

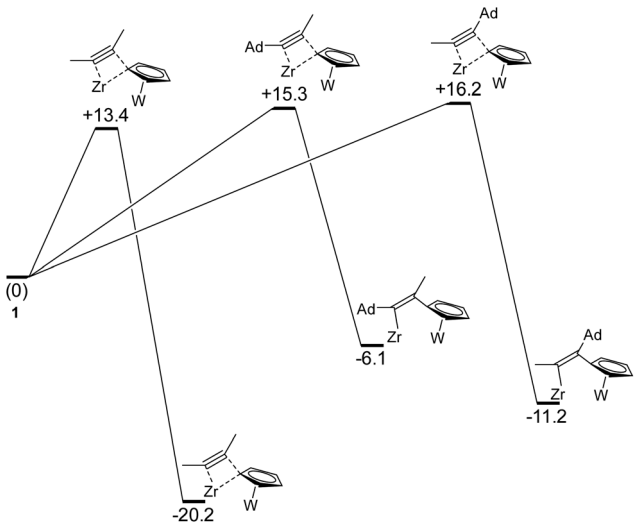

Fig. 11 Free energy profile for insertion of 2-butyne and methyl-adamantyl-acetylene.

Table 3 Barriers and reaction energies (kcal mol^{-1}) for alkyne and alkene insertion in **1**[a]

R^1/To Zr	R^2/To W	$\Delta G^{\ddagger}$	ΔG_{rxn}
	[Zr]–C(R^1)=C(R^2)–[W]		
H	H	n/a	−31.5
Me	Me	13.4	−20.2
Me	Ph	14.5	−19.4
Ph	Me	15.2	−19.7
Me	*t*Bu	16.5	−14.1
*t*Bu	Me	18.2	−6.8
Me	Ad	16.2	−11.2
Ad	Me	15.3	−6.1
*t*Bu	*t*Bu	29.1	+14.3
Ad	Ad	28.6	+17.7
	[Zr]–(R^1)–(R^2)–[W]		
CH_2	CH_2	14.4	−16.6
CH_2	CH*n*Bu	17.4	−14.3
CH*n*Bu	CH_2	22.0	−9.4
CH_2	CMe_2	19.3	−8.7
CMe_2	CH_2	28.9	−0.1
CMe_2	CMe_2	36.2	+12.6

[a] Free energies relative to separated **1** and alkyne/alkene.

In terms of bonding, alkyne adduct **7a**, perhaps surprisingly, shows a core arrangement similar to the symmetric inversion TS of **1**: Zr interacts comparably with both hydrides (0.059/0.079 e, see Table 2 and Fig. 12A and B). Presumably due to geometric constraints, the two hydrides are tilted out of the Zr coordination plane. This is not an ideal geometry for donation to Zr (although "mismatched" Cp_2WH_2 orientation has also been reported for a Cu(I) complex[59]), and perhaps due to this we find for complex **7a** a small amount of Zr mixing into the W LP (.046 e). Still, the overall pattern of dominant WH donation and relative inertness of the W lone pair seems to hold also for the alkyne adducts.

1-Hexene insertion was also checked. Consistent with the results for alkyne insertion, the lowest insertion barrier (17.1 kcal mol^{-1}, only slightly higher than alkyne insertion) is found for the hexene "bulk" (*n*Bu group) approaching the W centre. Hexene insertion is also exergonic enough to make it irreversible. To put this reaction in context, calculated energetics for insertion of ethene, isobutene and 2,3-dimethyl-2-butene are included in Table 3. The trend follows that of alkyne insertion, going from clearly exergonic (ethene) to highly endergonic (2,3-dimethyl-2-butene).

Correlations between structure and spectroscopic parameters

NMR spectroscopic parameters of transition metal hydrides are strongly affected by the electronic structure of the complex and M–H bonding situation.[66–69] Even though all hydrides reported in this work seem to follow the same bonding pattern, there is a discrete variability in their δ_H and $^1J_{WH}$ values (see above). By plotting the experimentally obtained δ_H *versus* the computed closest Zr–H distance in the bridging hydrides (Fig. 13a), a linear correlation is obtained (R = 0.89). Similarly, a rough linear correlation is also found between chemical shift values and optimised Zr–W distances (ESI†). The $^1J_{WH}$ values are instead less responsive and the data are much more scattered (linear fit R = 0.67, ESI†).

In the approximation that bond length reflects the interaction degree between the Zr centre and the hydride ligand, we could expect that stronger bridging interactions would affect more strongly the NMR observables. Generally, the smaller the

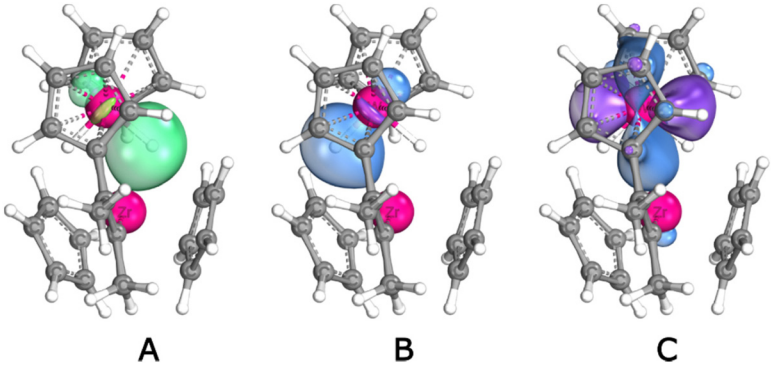

Fig. 12 IBOs for adduct **7a**: (A and B) the W–H bonds; (C) lone pair.

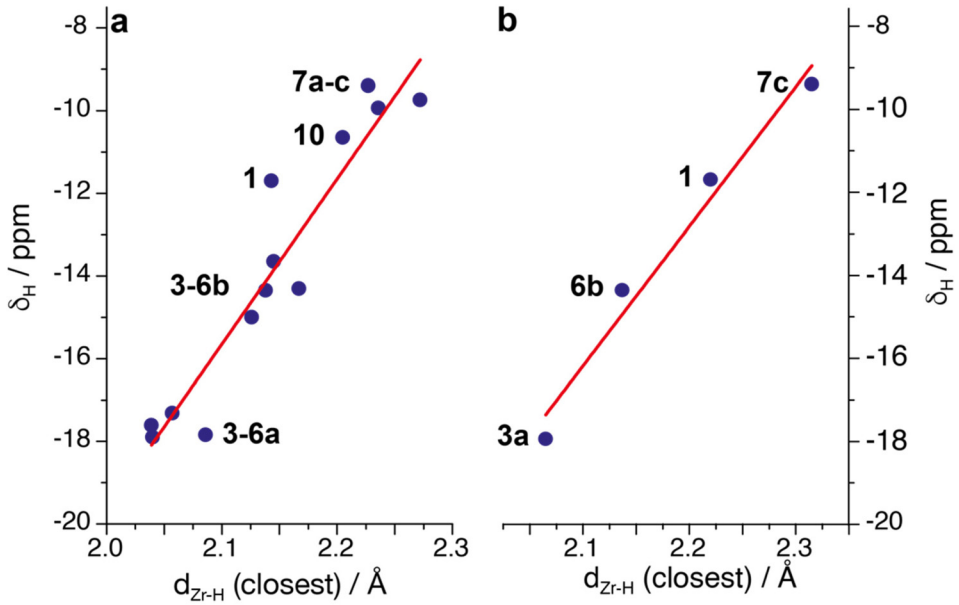

Fig. 13 (a) Plot of experimental chemical shift values *versus* the closest Zr–H distance obtained by DFT optimised structures in complexes **1–7**; (b) plot of chemical shift *versus* the approximate experimental Zr–H distances obtained by X Ray diffraction.

Zr–H distance in the bridging hydride, the more negative the δ_H and the lower the $^1J_{WH}$. The opposite trend is observed with the Zr–W distance: the higher the intermetallic separation, the lower the hydride δ_H. The same linear trend was obtained also when δ_H values were plotted against the experimentally available Zr–H distances (Fig. 13b). Even though the presumed large uncertainty of the experimental M–H determination must be considered, there is good agreement with the theoretical data.

Given that δ_H values are averaged between bridging and non-bridging hydrides by their very fast interconversion at RT, the validity of this correlation over a range of 8 ppm is remarkable. The lower chemical shift at shorter Zr–H distances seems to fit with the general rule of thumb that bridging group IV metallocene hydrides are more shielded than the corresponding terminal ones. It is likely that the weak overlap between W–H and Zr empty orbitals described above may increase the paramagnetic shielding contribution[70] or enhance the effect of spin–orbit coupling, as previously observed by some of us in Cp_2WH_2/Au(III) bridging hydrides.[25]

Irrespective of the quantum mechanical origin of such an effect, we can use this correlation to categorise all the complexes synthesised in this work. From the data reported in Fig. 13a, three main clusters of compounds can be identified: (i) the *outside* Lewis adducts, with Zr–H distances between 2.0 and 2.1 Å and δ_H around −18 ppm, (ii) the *inside* Lewis adducts (Zr–H 2.1 to 2.2 Å, δ_H *ca.* −15 to −14 ppm) and (iii) the alkyne/alkene insertion products (Zr–H over 2.2 Å, δ_H *ca.* −10 to −9 ppm). Complex **1** seems to fall in between class (ii) and class (iii), even though it fits better the experimental trend than the theoretical one. Such a linear response of δ_H for the whole series is a clear sign that minor alterations in the geo-

metry of the adducts lead to a fine tuning of the Zr–H–W bridge, which can be assessed by simply using the ^{1}H NMR chemical shift of the hydride atom.

Conclusion

Reactions of zirconocene alkyl cations with Lewis basic Cp_2WH_2 lead to the formation of the bridging hydride $[Cp_2Zr(\mu\text{-}H)(\mu\text{-}\eta^1\text{:}\eta^5\text{-}C_5H_4)WHCp]^+$ (**1**) upon σ-bond metathesis of one W–Cp ring. **1** is characterised by an unusual out of plane bridging hydride interaction, which makes the core of the complex very flexible. The thermodynamically preferred asymmetric configuration is in fast interconversion with a symmetric arrangement, with a calculated barrier of <2 kcal mol^{-1}. Despite being floppy, the bridging interaction in **1** is not broken by other ligands. **1** reacts, indeed, with Lewis bases affording adducts where the bridging hydride is either close (*W-inside*) or opposite to the coordinated base (*W-outside*). With PMe_3, the latter is preferred while with other more labile bases, such as $Ptol_3$, THF or 3,5-lutidine, the *inside* configuration is obtained almost exclusively. In forming such adducts, the bridging hydride switches to an in-plane configuration and the average Zr–H distances decrease with respect to **1**.

Despite the proximity between the Lewis acidic Zr and the lone pair of W, reactions of **1** with alkynes, alkenes and H_2 proceed without any bimetallic cooperativity. In reacting with unactivated internal alkynes and olefins, insertion proceeds selectively into the Zr–C bond leading to vinyl or alkyl-metallocene complexes. In these species, the hydrides still interact with the Zr centre, but assume a perpendicular orientation with respect to its coordination plane. With H_2, a trimetallic complex is obtained upon σ-bond metathesis of the H–H bond.

DFT studies revealed that metal–metal interactions in all these species are negligible, and the lone pair remains localised on tungsten. On the other hand, considerable overlap between W–H and Zr empty orbitals is observed, suggesting that the most reasonable description of these species is an "open" 3c2e bonding interaction. The computed Zr–H bond distances correlate linearly with the experimentally observed ^{1}H chemical shift values of the hydrides, indicating that NMR parameters can be used to assess the proximity of the bridging hydride to the Zr centre.

The results reported above strongly point to the fact that short metal–metal distances in the solid state or hydride ^{1}H NMR trends in solution should not be used as univocal parameters to imply the presence of an M–M bond in heterobimetallic dihydrides. Moreover, very small alterations in the coordination environment of these complexes modulate the degree of interaction between the W–H bond and the Zr centre, with important effects on reactivity, as it is shown in the case of hydrogenolysis. We are currently trying to introduce further modifications in this class of compounds aiming at triggering bimetallic cooperation in small molecule activation and enable novel reactivity in zirconocene chemistry.

Experimental section

Materials and methods

All manipulations of air-sensitive materials were performed in flamed Schlenk glassware on a Schlenk line or in nitrogen-filled Mbraun Unilab gloveboxes with a high-capacity recirculator (<1 ppm O_2 and H_2O). Deuterated solvents were freeze–pump–thaw degassed, distilled over the appropriate drying agent (CaH_2 or Na/K alloy), and stored over activated 4 Å molecular sieves in the glovebox.

Cp_2ZrMe_2 [71] and $B(C_6F_5)_3$ [72] were synthesized according to literature procedures. $[HNMe_2Ph][B(C_6F_5)_4]$ was purchased from Strem and used as received. Cp_2WH_2 was purchased from Sigma Aldrich and further purified by vacuum sublimation when required. Trimethylphosphine (1 M in THF, Sigma Aldrich) was used as received. Tris-*para*-tolylphosphine and 3,5-lutidine (Sigma Aldrich) were dried under vacuum and stored in the glovebox. 2-Butyne, 4-4′-dimethyl-2-pentyne (Alfa Aesar), dimethylacetylene dicarboxylate, 1-phenylpropyne, and 1-hexene (Sigma Aldrich) were freeze–pump–thawed degassed and stored over activated 4 Å molecular sieves in the glovebox.

Experiments with H_2 were performed in J-Young NMR tubes on a dedicated Schlenk line interfaced with a H_2 gas supply (>99.5% purity) at 1 atmosphere. In the typical procedure, NMR solutions were initially freeze–pump–thaw degassed three times to remove the headspace. Successively, H_2 was introduced in the NMR tube at −78 °C and the solution was left to equilibrate at the desired temperature.

^{1}H, ^{19}F, ^{31}P{^{1}H}, ^{13}C{^{1}H}, ^{1}H NOESY, ^{1}H,^{13}C HMQC, ^{1}H,^{13}C HSQC, ^{1}H,^{13}C HMBC, ^{19}F,^{1}H HOESY NMR experiments have been recorded on Bruker Avance III HD 400 and Bruker DPX-300 spectrometers equipped with ^{1}H, BB smartprobes and *Z*-gradients. ^{1}H NMR spectra are referenced to residual protons of the deuterated solvent. ^{13}C NMR spectra are referenced to the D-coupled ^{13}C signals of the solvent. ^{19}F NMR are referenced to an external standard of $CFCl_3$. ^{31}P NMR are referenced to an external standard of H_3PO_4.

Crystallographic details

CCDC 2212595–2212600† contain the supplementary crystallographic data for this paper.

DFT calculations

DFT calculations were performed using Gaussian 16[73] coupled to an external optimizer.[74] All structures were fully optimised, without constraints or symmetry restrictions, as minima or transition states, using the dispersion-aware functional MN15[75] and the cc-pVDZ(PP) basis set.[76–79] Analytical frequency calculations were done to check the nature of all stationary points (minima without imaginary frequencies, transition states with exactly one with the correct movement). IRC calculations failed in several cases for the flat energy surfaces associated with cluster rearrangement, so connectivity of each transition state was checked by moving each TS along the reaction coordinate (in both directions, 0.03 to 0.20 Bohr) and re-optimizing. Thermal corrections (enthalpy and entropy) at 298 K were calculated from the

vibrational analyses and were scaled by 0.67 to account for reduced freedom in solution.[80,81] Improved single-point energies were calculated at the MN15/cc-pVTZ(PP) level including a solvent (benzene) correction using the SMD model,[82] and were combined with the thermal corrections to obtain final free energies; all energies mentioned in the text are Gibbs free energies. Optimisations including the solvent model were also attempted, but in many cases these were found to fail spectacularly due to gradient discontinuities apparently caused by discretization issues. In any case, the solvent used here (benzene) is not very polar and is not expected to affect the results much.

The "intrinsic bond orbital" formalism introduced by Knizia[64,65] was used to analyse bonding in the bimetallic cores of Zr/W bimetallic complexes. IBOview was used to calculate (exponent: 4) IBOs from the MN15/cc-pVDZ(PP) wave functions that were produced by Gaussian and converted to Molden[83] format.

Data availability

Experimental details, NMR spectra, crystallographic and DFT details are collected in the Electronic ESI.†

Conflicts of interest

There are no conflicts to declare.

Acknowledgements

LR acknowledges the University of East Anglia and the Royal Society of Chemistry (R21-1292108967) for financial support. We thank MIUR (AMIS, "Dipartimenti di Eccellenza 2018–2022" program). We also thank the UK National Crystallography Service[84] for the acquisition of crystallographic data of **1B(C$_6$F$_5$)$_4$**, **2**, **7a** and **10**, while Dr Leonardo Tensi (University of Perugia) is acknowledged for assistance with the X-Ray structures of **3a** and **6b**.

References

1 L. M. Venanzi, *Coord. Chem. Rev.*, 1982, **43**, 251–274.
2 J. Campos, *Nat. Rev. Chem.*, 2020, **4**, 696–702.
3 M. Navarro and J. Campos, in *Advances in Organometallic Chemistry*, Academic Press Inc., 2021, vol. 75, pp. 95–148.
4 B. G. Cooper, J. W. Napoline and C. M. Thomas, *Catal. Rev.: Sci. Eng.*, 2012, **54**, 1–40.
5 E. Bodio, M. Picquet and P. le Gendre, in *Homo- and Heterobimetallic Complexes in Catalysis: Cooperative Catalysis*, ed. P. Kalck, Springer International Publishing, Cham, 2015, pp. 139–186.
6 G. G. Hlatky and R. H. Crabtree, *Coord. Chem. Rev.*, 1985, **65**, 1–48.
7 M. D. Fryzuk, J. B. Love, S. J. Rettig and V. G. Young, *Science*, 1997, **275**, 1445–1447.
8 X. Zhao, I. P. Georgakaki, M. L. Miller, R. Mejia-Rodriguez, C. Y. Chiang and M. Y. Darensbourg, *Inorg. Chem.*, 2002, **41**, 3917–3928.
9 J. C. Green, M. L. H. Green and G. Parkin, *Chem. Commun.*, 2012, **48**, 11481–11503.
10 R. E. Adams, T. A. Grusenmeyer, A. L. Griffith and R. H. Schmehl, *Coord. Chem. Rev.*, 2018, **362**, 44–53.
11 A. Maity and T. S. Teets, *Chem. Rev.*, 2016, **116**, 8873–8911.
12 R. N. Perutz and B. Procacci, *Chem. Rev.*, 2016, **116**, 8506–8544.
13 S. M. Baldwin, J. E. Bercaw, L. M. Henling, M. W. Day and H. H. Brintzinger, *J. Am. Chem. Soc.*, 2011, **133**, 1805–1813.
14 S. M. Baldwin, J. E. Bercaw and H. H. Brintzinger, *J. Am. Chem. Soc.*, 2010, **132**, 13969–13971.
15 S. M. Baldwin, J. E. Bercaw and H. H. Brintzinger, *J. Am. Chem. Soc.*, 2008, **130**, 17423–17433.
16 A. M. Baranger and R. G. Bergman, *J. Am. Chem. Soc.*, 1994, **116**, 3822–3835.
17 M. J. Butler, A. J. P. White and M. R. Crimmin, *Organometallics*, 2018, **37**, 949–956.
18 M. J. Butler, A. J. P. White and M. R. Crimmin, *Angew. Chem., Int. Ed.*, 2016, **55**, 6951–6953.
19 J. W. Bruno, J. C. Huffman, M. A. Green and K. G. Caulton, *J. Am. Chem. Soc.*, 1984, **106**, 8310–8312.
20 M. Oishi and H. Suzuki, *Inorg. Chem.*, 2009, **48**, 2349–2351.
21 A. Berry, M. L. H. Green, J. A. Bandy and K. Prout, *J. Chem. Soc., Dalton Trans.*, 1991, 2185–2206.
22 V. I. Bakhmutov, M. Visseaux, D. Baudry, A. Dormond and P. Richard, *Inorg. Chem.*, 1996, **35**, 7316–7324.
23 G. Parkin, *Metal-metal bonding in bridging hydride and alkyl compounds*, 2010, vol. 136.
24 J. W. Lauher and R. Hoffmann, *J. Am. Chem. Soc.*, 1976, **98**, 1729–1742.
25 L. Rocchigiani, W. T. Klooster, S. J. Coles, D. L. Hughes, P. Hrobárik and M. Bochmann, *Chem. – Eur. J.*, 2020, **26**, 8267–8280.
26 J. W. Bruno, J. C. Huffman and K. G. Caulton, *J. Am. Chem. Soc.*, 1984, **106**, 444–445.
27 H. Brunner and D. Mijolovic, *J. Organomet. Chem.*, 1999, **577**, 346–350.
28 A. Albinati, R. Naegeli, A. Togni and L. M. Venanzi, *Organometallics*, 2002, **2**, 926–928.
29 H. Brunner, M. Muschiol, T. Neuhierl and B. Nuber, *Chem. – Eur. J.*, 1998, **4**, 168–171.
30 X. Yang, C. L. Stern and T. J. Marks, *J. Am. Chem. Soc.*, 1994, **116**, 10015–10031.
31 L. Rocchigiani, G. Ciancaleoni, C. Zuccaccia and A. Macchioni, *Angew. Chem., Int. Ed.*, 2011, **50**, 11752–11755.
32 L. Rocchigiani, G. Bellachioma, G. Ciancaleoni, A. Macchioni, D. Zuccaccia and C. Zuccaccia, *Organometallics*, 2010, **30**, 100–114.
33 A. D. Horton and J. de With, *Organometallics*, 1997, **16**, 5424–5436.
34 R. Waterman, *Organometallics*, 2013, **32**, 7249–7263.
35 B. Cordero, V. Gómez, A. E. Platero-Prats, M. Revés, J. Echeverría, E. Cremades, F. Barragán and S. Alvarez, *J. Chem. Soc., Dalton Trans.*, 2008, 2832–2838.

36 A. Bartole-Scott, A. J. Lough and I. Manners, *Polyhedron*, 2006, **25**, 429–436.
37 C. P. Casey, R. E. Palermo, R. F. Jordan and A. L. Rheingold, *J. Am. Chem. Soc.*, 1985, **107**, 4597–4599.
38 A. Ramos, E. Otten and D. W. Stephan, *J. Am. Chem. Soc.*, 2009, **131**, 15610–15611.
39 D. Takeuchi, J. Kuwabara and K. Osakada, *Organometallics*, 2003, **22**, 2305–2311.
40 A. Albinati, A. Togni and L. M. Venanzi, *Organometallics*, 1986, **5**, 1785–1791.
41 O. W. Howarth, C. H. McAteer, P. Moore, G. E. Morris and N. W. Alcock, *J. Chem. Soc., Dalton Trans.*, 1982, 541–548.
42 N. S. Radu, P. K. Gantzel and T. D. Tilley, *J. Chem. Soc., Chem. Commun.*, 1994, 1175–1176.
43 F. Hannig, R. Fröhlich, K. Bergander, G. Erker and J. L. Petersen, *Organometallics*, 2004, **23**, 4495–4502.
44 H. Braunschweig and C. Kollann, *Z. Naturforsch., B: J. Chem. Sci.*, 1999, **54**, 839–842.
45 L. Sian, A. Dall'Anese, A. Macchioni, L. Tensi, V. Busico, R. Cipullo, G. P. Goryunov, D. Uborsky, A. Z. Voskoboynikov, C. Ehm, L. Rocchigiani and C. Zuccaccia, *Organometallics*, 2022, **41**, 547–560.
46 Reactions with $\mathbf{1B(C_6F_5)_4}$ gave the same outcome.
47 K. Yan, A. Pindwal, A. Ellern and A. D. Sadow, *Dalton Trans.*, 2014, **43**, 8644–8653.
48 R. F. Jordan, C. S. Bajgur, W. E. Dasher and A. L. Rheingold, *Organometallics*, 1987, **6**, 1041–1051.
49 M. Dahlmann, R. Fröhlich and G. Erker, *Eur. J. Inorg. Chem.*, 2000, **2000**, 1789–1793.
50 A. D. Miller, S. A. Johnson, K. A. Tupper, J. L. McBee and T. D. Tilley, *Organometallics*, 2009, **28**, 1252–1262.
51 V. H. Gessner, J. F. Tannaci, A. D. Miller and T. D. Tilley, *Acc. Chem. Res.*, 2011, **44**, 435–446.
52 G. E. Herberich and W. Barlage, *Organometallics*, 1987, **6**, 1924–1930.
53 P. H. M. Budzelaar, D. L. Hughes, M. Bochmann, A. Macchioni and L. Rocchigiani, *Chem. Commun.*, 2020, **56**, 2542–2545.
54 P. Legzdins, J. T. Martin, F. W. B. Einstein and A. C. Willis, *J. Am. Chem. Soc.*, 2002, **108**, 7971–7981.
55 F. Wu and R. F. Jordan, *Organometallics*, 2005, **24**, 2688–2697.
56 M. P. Johnson and D. F. Shriver, *J. Am. Chem. Soc.*, 1966, **88**, 301–304.
57 J. W. Bruno, J. C. Huffman and K. G. Caulton, *J. Am. Chem. Soc.*, 1984, **106**, 444–445.
58 M. P. Johnson and D. F. Shriver, *J. Am. Chem. Soc.*, 1966, **88**, 301–304.
59 A. Hicken, A. J. P. White and M. R. Crimmin, *Dalton Trans.*, 2018, **47**, 10595–10600.
60 M. Amati and F. Lelj, *Can. J. Chem.*, 2009, **87**, 1406–1414.
61 H. Brunner, A. Hollman and M. Zabel, *J. Organomet. Chem.*, 2001, **630**, 169–176.
62 H. Brunner, M. Muschiol, T. Neuhierl and B. Nuber, *Z. Naturforsch., B: J. Chem. Sci.*, 1999, **54**, 337–340.
63 H. Brunner, A. Hollman, B. Nuber and M. Zabel, *J. Organomet. Chem.*, 2001, **633**, 1–6.
64 G. Knizia, *J. Chem. Theory Comput.*, 2013, **9**, 4834–4843.
65 G. Knizia and J. E. M. N. Klein, *Angew. Chem., Int. Ed.*, 2015, **54**, 5518–5522.
66 L. Rocchigiani, J. Fernandez-Cestau, I. Chambrier, P. Hrobárik and M. Bochmann, *J. Am. Chem. Soc.*, 2018, **140**, 8287–8302.
67 L. Rocchigiani, P. H. M. Budzelaar and M. Bochmann, *Chem. Sci.*, 2019, **10**, 2633–2642.
68 Z.-L. Xue, T. M. Cook and A. C. Lamb, *J. Organomet. Chem.*, 2017, **852**, 74–93.
69 P. Hrobárik, V. Hrobáriková, F. Meier, M. Repiský, S. Komorovský and M. Kaupp, *J. Phys. Chem. A*, 2011, **115**, 5654–5659.
70 Y. Ruiz-Morales, G. Schreckenbach and T. Ziegler, *Organometallics*, 1996, **15**, 3920–3923.
71 E. Samuel and M. D. Rausch, *J. Am. Chem. Soc.*, 1973, **95**, 6263–6267.
72 S. J. Lancaster, *ChemSpider* DOI: **10.1039/SP215**.
73 M. J. Frisch, G. W. Trucks, H. B. Schlegel, G. E. Scuseria, M. A. Robb, J. R. Cheeseman, G. Scalmani, V. Barone, G. A. Petersson, H. Nakatsuji, X. Li, M. Caricato, A. v Marenich, J. Bloino, B. G. Janesko, R. Gomperts, B. Mennucci, H. P. Hratchian, J. v Ortiz, A. F. Izmaylov, J. L. Sonnenberg, D. Williams-Young, F. Ding, F. Lipparini, F. Egidi, J. Goings, B. Peng, A. Petrone, T. Henderson, D. Ranasinghe, V. G. Zakrzewski, J. Gao, N. Rega, G. Zheng, W. Liang, M. Hada, M. Ehara, K. Toyota, R. Fukuda, J. Hasegawa, M. Ishida, T. Nakajima, Y. Honda, O. Kitao, H. Nakai, T. Vreven, K. Throssell, J. A. Montgomery, Jr., J. E. Peralta, F. Ogliaro, M. J. Bearpark, J. J. Heyd, E. N. Brothers, K. N. Kudin, V. N. Staroverov, T. A. Keith, R. Kobayashi, J. Normand, K. Raghavachari, A. P. Rendell, J. C. Burant, S. S. Iyengar, J. Tomasi, M. Cossi, J. M. Millam, M. Klene, C. Adamo, R. Cammi, J. W. Ochterski, R. L. Martin, K. Morokuma, O. Farkas, J. B. Foresman and D. J. Fox, Gaussian, Inc., Wallingford CT.
74 P. H. M. Budzelaar, *J. Comput. Chem.*, 2007, **28**, 2226–2236.
75 H. S. Yu, X. He, S. L. Li and D. G. Truhlar, *Chem. Sci.*, 2016, **7**, 5032–5051.
76 B. P. Pritchard, D. Altarawy, B. Didier, T. D. Gibson and T. L. Windus, *J. Chem. Inf. Model.*, 2019, **59**, 4814–4820.
77 T. H. Dunning, *J. Chem. Phys.*, 1989, **90**, 1007–1023.
78 K. A. Peterson, D. Figgen, M. Dolg and H. Stoll, *J. Chem. Phys.*, 2007, **126**, 124101.
79 D. Figgen, K. A. Peterson, M. Dolg and H. Stoll, *J. Chem. Phys.*, 2009, **130**, 164108.
80 R. Raucoules, T. de Bruin, P. Raybaud and C. Adamo, *Organometallics*, 2009, **28**, 5358–5367.
81 S. Tobisch and T. Ziegler, *J. Am. Chem. Soc.*, 2004, **126**, 9059–9071.
82 J. B. Foresman, T. A. Keith, K. B. Wiberg, J. Snoonian and M. J. Frisch, *J. Phys. Chem.*, 1996, **100**, 16098–16104.
83 G. Schaftenaar and J. H. Noordik, *J. Comput.-Aided Mol. Des.*, 2000, **14**, 123–134.
84 S. J. Coles and P. A. Gale, *Chem. Sci.*, 2012, **3**, 683–689.

